Physics of the Earth and Planetary Interiors 312 (2021) 106674

Contents lists available at ScienceDirect

Physics of the Earth and Planetary Interiors

journal homepage: www.elsevier.com/locate/pepi

A moment tensor inversion approach based on the correlation between defined functions and waveforms

Yue Kong [a], Min Li [a], Weimin Chen [b,c,*], Ning Liu [d], Boqi Kang [e]

[a] School of Aeronautic Science and Engineering, Beihang University, Beijing 100083, China
[b] Institute of Mechanics, Chinese Academy of Sciences, Beijing 100190, China
[c] School of Engineering Science, University of Chinese Academy of Sciences, Beijing 100049, China
[d] College of Mechanical and Electrical Engineering, Beijing University of Chemical Technology, Beijing 100029, China
[e] Key Laboratory of Space Utilization, Technology and Engineering Center for Space Utilization, Chinese Academy of Sciences, Beijing 100094, China

ARTICLE INFO

Keywords:
Moment tensor
Correlation
Noise
Multiple sources

ABSTRACT

The moment tensor inversion is a commonly-used method to interpret source mechanisms of microseismicity. In the inversion for real data (e.g. microseismicity recorded during hydraulic fracturing), the waveforms recorded by sensors can be the mixtures of signals and noise, or the superposition of signals generated by multiple sources. Then the traditional approach may result in inaccurate solutions. In this article, we developed a new inversion approach based on the correlation between waveforms and correlation functions, which are defined based on the characteristics of signals. The correlation function determined by specific parameters is more sensitive to the signal generated by a specific source, and less sensitive to noise or signals generated by other sources. Then the correlation coefficient calculated by multiplying the waveform and correlation function is mainly determined by the signal. The moment-tensor solutions calculated by the correlation coefficients are more accurate. The new inversion approach was evaluated by synthetic tests. For noise filtering, compared with tradition inversion approaches, the new approach can improve the inversion accuracy by more than 50% at various noise levels. For multiple sources discrimination, the new approach can discriminate signals generated by multiple sources and provide more accurate inversion results for the sources simultaneously, but the application of the method is limited. This new inversion approach aims to provide accurate solutions in a very simple way, when the waveforms are distorted.

1. Introduction

The properties of microseismic sources is quite helpful for understanding the evolution of stress filed (Van Der Baan et al., 2016; Eaton et al., 2014) and evaluating the performance of hydraulic fracturing treatments (Baig and Urbancic, 2010; Eyre and Van Der Baan, 2015). One commonly-used method to interpret source mechanisms is the moment tensor inversion. A moment tensor represents a group of equivalent forces acting at the position of a seismic source and can be recovered by seismic waves recorded by sensors. Then a decomposition approach can be used to extract the information from moment tensors and the source properties can be obtained.

The moment tensor inversion is originally proposed to monitor earthquakes. As early as 1964, Burridge and Knopoff (1964) derived the expression of body forces to be applied in the absence of a dislocation. Then Aki and Richards (2002) provided detailed derivations of moment tensors and the inversion equations. The moment tensor of a seismic source can be calculated by wave amplitudes (Fojtíková et al., 2010; Vavryčuk et al., 2008), amplitude ratios (Hardebeck and Shearer, 2003; Jechumtalova and Silený, 2005) and full waveforms (Dziewonski et al., 1981; Silený et al., 1992; Sipkin, 1986). Among the three methods, the amplitude method can provide relatively accurate solutions by a relatively simple inversion approach and is widely used for various engineering applications. After retrieving moment tensors, the seismic sources can be physically interpreted by the decomposition of moment tensors into three basic components (Vavryčuk, 2015), which are commonly isotropic (ISO), double-couple (DC) and compensated linear vector dipole (CLVD). In order to visually illustrate source types, the

* Corresponding author at: Institute of Mechanics, Chinese Academy of Sciences, Beijing 100190, China; School of Engineering Science, University of Chinese Academy of Sciences, Beijing 100049, China.
E-mail address: wmchen@imech.ac.cn (W. Chen).

https://doi.org/10.1016/j.pepi.2021.106674
Received 29 August 2020; Received in revised form 4 February 2021; Accepted 5 February 2021
Available online 9 February 2021

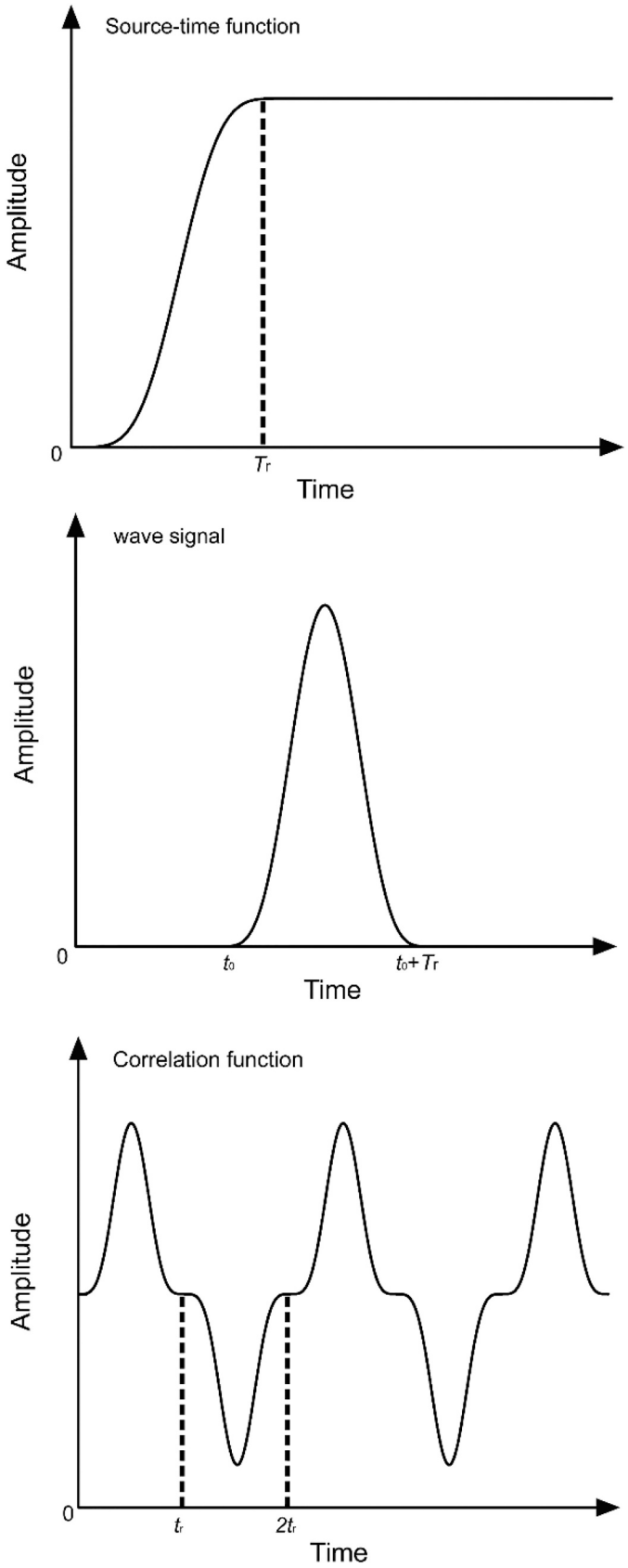

Fig. 1. Source-time function, wave signal and correlation function. T_r is the rise time of source-time functions. t_r is the duration time of correlation functions.

source-type plots are also provided (Hudson et al., 1989; Tape and Tape, 2012; Vavryčuk, 2015). Now the moment tensor inversion has been proved to be a powerful tool to interpret the source mechanisms of seismicity (Hejrani et al., 2017; Kanamori and Given, 1981; Napoli and Ebel, 2018; Sipkin, 1982). Because the source mechanisms of microseismicity and acoustic emission (AE) events are quite similar to that of seismicity, the inversion approach is also used for the corresponding applications (Fischer and Guest, 2011; Jechumtalova and Eisner, 2008; Xu et al., 2017; Zhang and Zhang, 2017).

The application of the moment tensor inversion to microseismicity is challenged and the inversion accuracy is seriously influenced by noise, which can be caused by several factors. First, the noise can be introduced by measurement and method errors (Mustac and Tkalcic, 2017). Second, the inaccuracy of velocity models can lead to unpredictable changes to waveforms. In addition, the waveforms recorded by sensors can be the mixture of signals generated by multiple sources (Vavrycuk et al., 2017). In this case, the first signal was distorted by the second signal and the

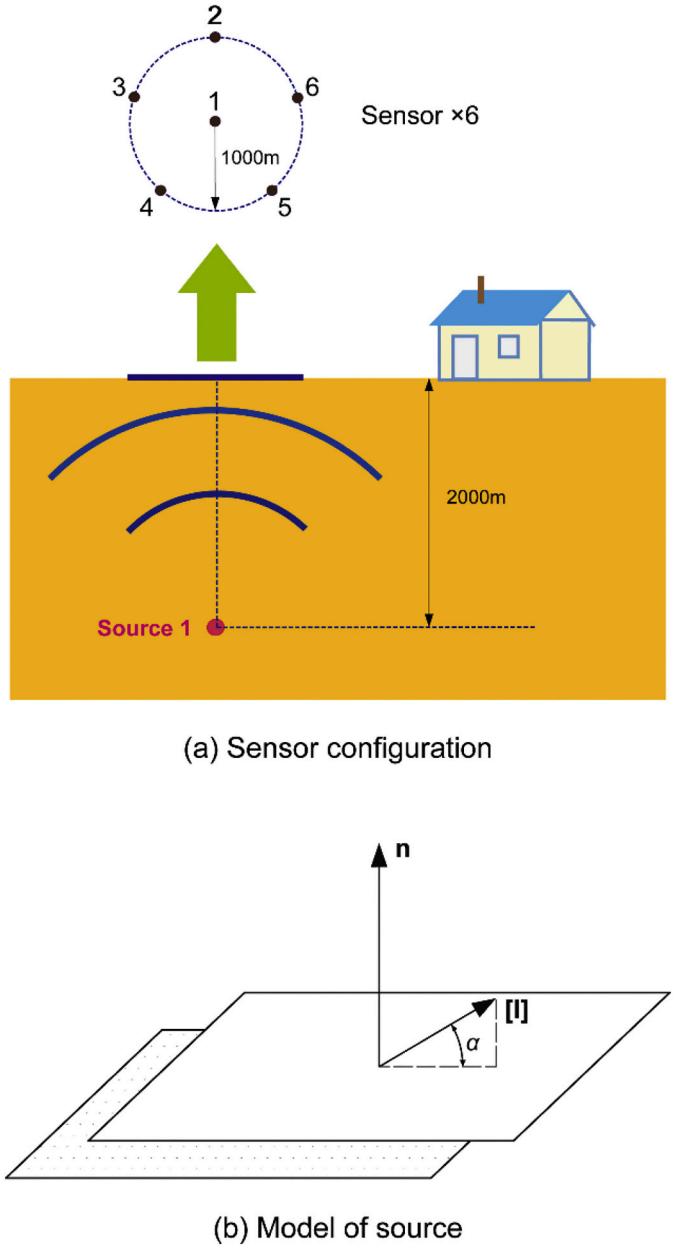

Fig. 2. (a) Relative positions between the sensors and source, (b) model of the source.

Table 1
Material parameters in synthetic tests.

Parameter	Elastic module	Poisson ratio	Density	P-wave velocity
Value	5.4×10^{10} Pa	0.2	2300 kg/m^3	5108 m/s

second signal can be regarded as the noise for the first source, and vice versa. In some cases, the effects of noise can be significantly reduced by removing noise. Specifically, noise can be filtered based on the difference of spectra between singles and noise (Cesca et al., 2006; Nakano et al., 2008; Vavryčuk and Kühn, 2012), or the waveforms contaminated by noise seriously can be discarded directly based on signal-to-noise levels (Birialtsev et al., 2017; Hallo et al., 2017; Jian et al., 2018). Alternatively, methods can be used to quantify the uncertainty generated by the noise and the inversion results containing uncertainty can still be used (Gu et al., 2017; Vackar et al., 2017).

Although the methods mentioned above are effective for some engineering applications, they are complex and computationally demanding. In this paper, we introduced a simple inversion approach based on the correlation theory. Correlation functions are defined based on the characteristics of signals, then the correlation coefficients calculated by the correlation functions and waveforms are sensitive to signals and insensitive to noise. Then the moment tensor inversion based on the correlation coefficients is less sensitive to noise and can achieve better inversion accuracy. In addition, the correlation functions of different parameters are sensitive to signals generated by different sources respectively, then the corresponding correlation coefficients are related to different sources. By the use of those correlation coefficients to invert for different sources, the accurate moment-tensor solutions of multiple sources can be obtained simultaneously. This new inversion approach is tested by synthetic seismic data to validate its performance of suppressing the effect of noise and discriminating multiple sources.

2. Formulas

2.1. Review of standard moment tensor inversion approach

In isotropic and homogeneous media, the moment-tensor components are expressed according to Vavryčuk and Hrubcová (2017) as:

$$M_{pq} = \left(\lambda l_k n_k \delta_{pq} + \mu l_p n_q + \mu l_q n_p\right) S_f, \tag{1}$$

where $p = 1, 2, 3$ and $q = 1, 2, 3$ represent X, Y, Z directions, λ and μ are the Lame constants, δ_{pq} is 1 while $p = q$, otherwise is 0, l_q are the components of the slip vector at the crack surfaces, and n_p are the components of the normal vector to the crack surfaces. S_f is the crack size.

Each moment-tensor component M_{pq} has the dimension of moment and represents a force couple acting at the positons of cracks. According to Eq. (1), nine components can be obtained for a crack and orderly arranged in a 3×3 matrix notion. In addition, 6 of the 9 components are independent and require at least 6 sensors in the inversion to avoid an underdetermined problem.

In isotropic and homogeneous media, the compressional waves (P wave) generated by a source with moment tensor **M** can be expressed according to Aki and Richards (2002) as:

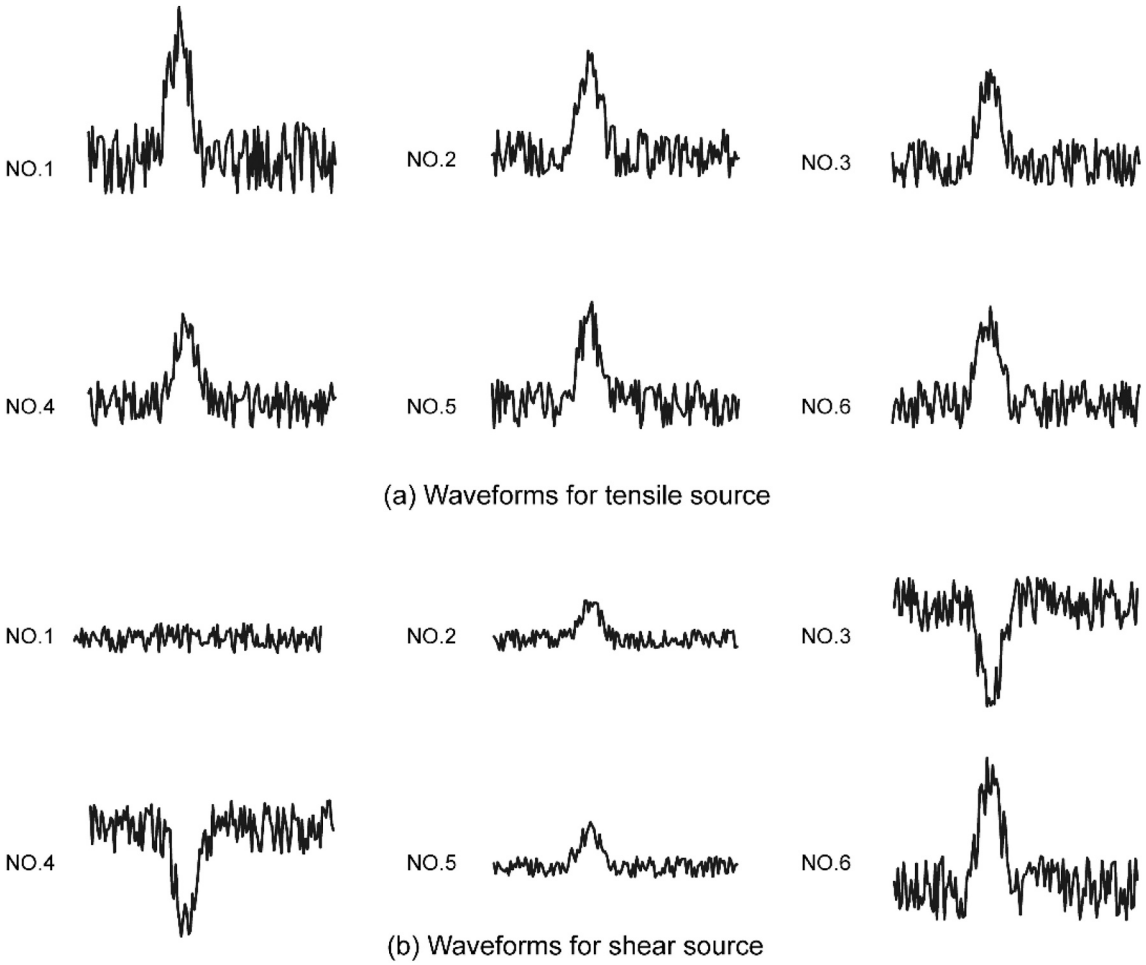

Fig. 3. Distorted waveforms for the noise level of 30%.

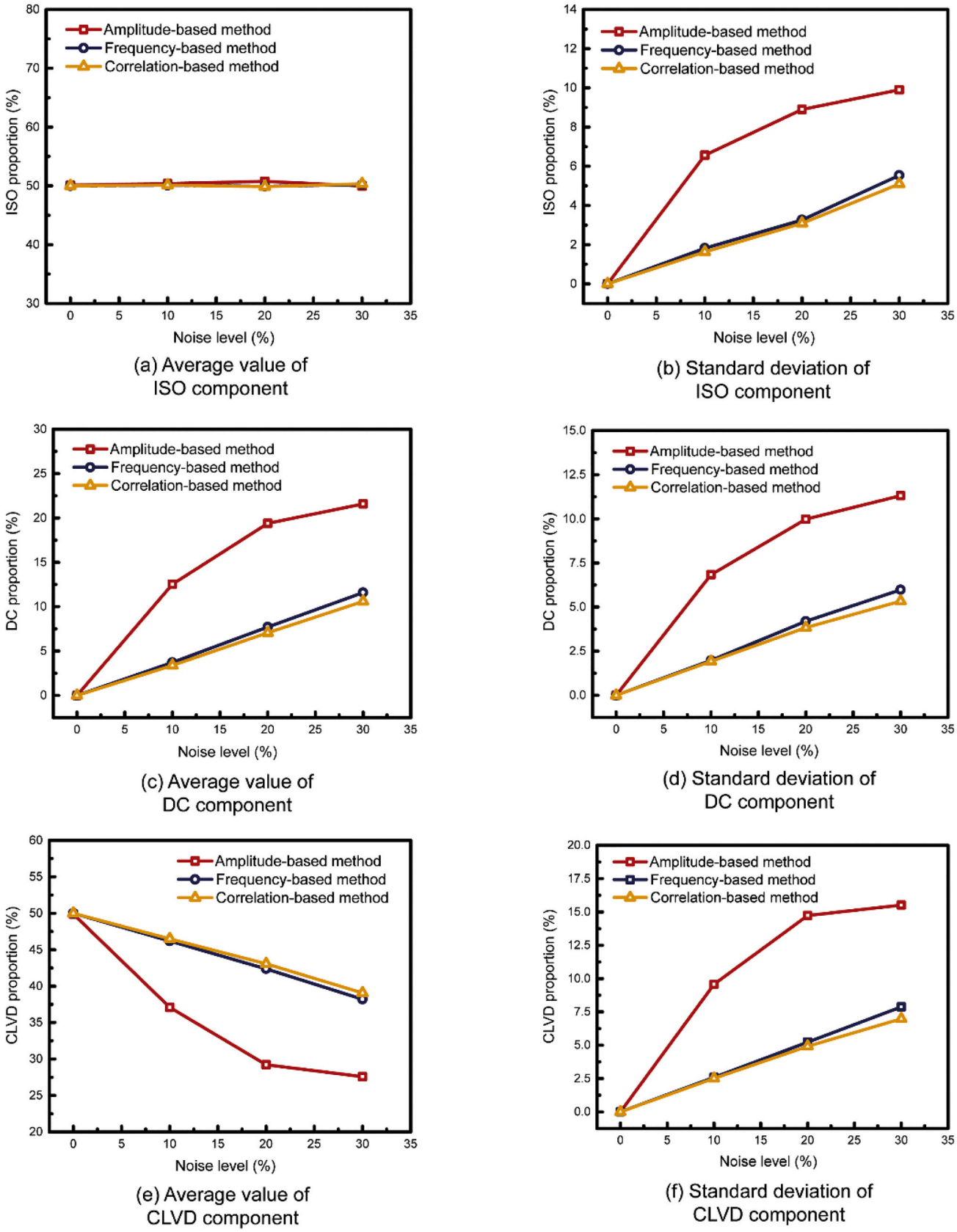

Fig. 4. For tensile cracks, inversion results of ISO, DC and CLVD components for the three methods at four noise levels. The synthetic tests at one noise level for one method are repeated by 100 times and the average values and standard deviations of the results are plotted. The correct values of ISO, DC and CLVD proportions are 50%, 0 and 50% respectively.

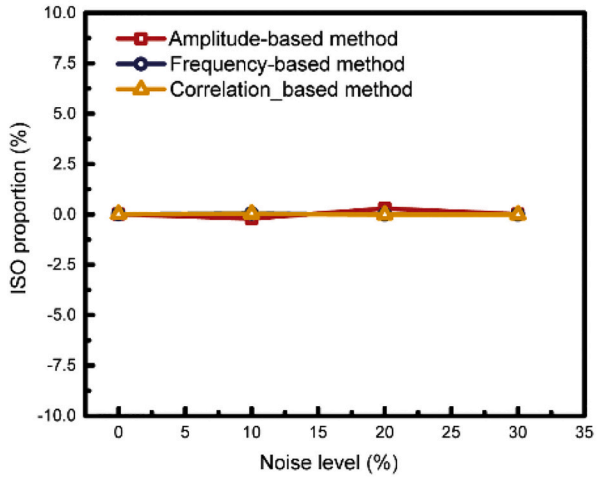

(a) Average value of ISO component

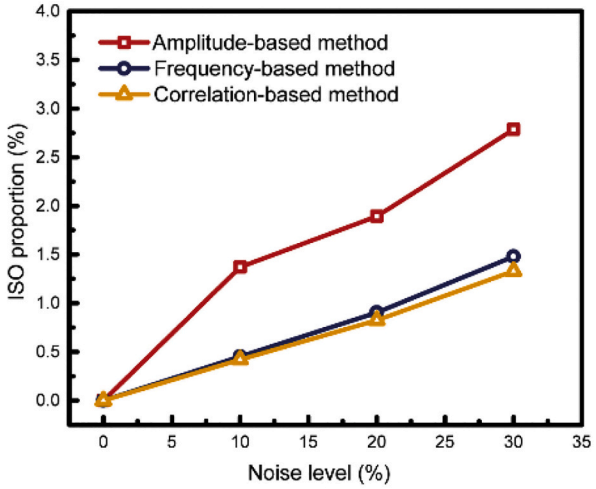

(b) Standard deviation of ISO component

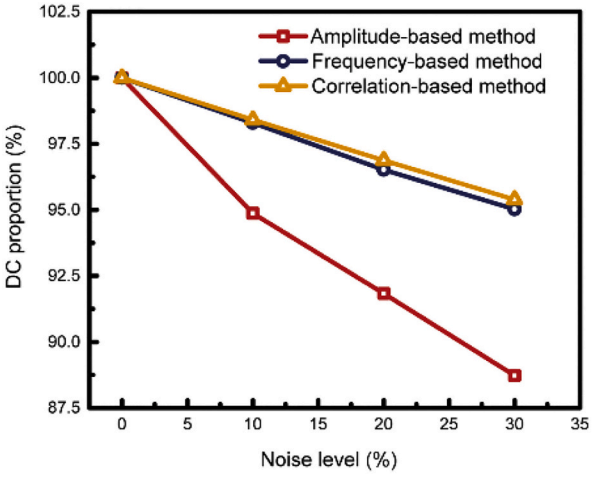

(c) Average value of DC component

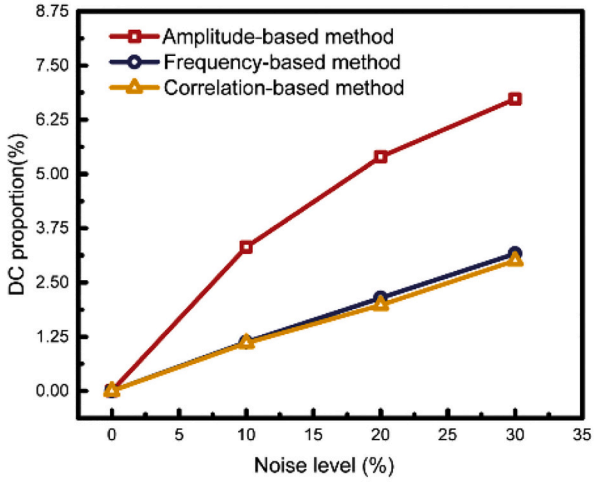

(d) Standard deviation of DC component

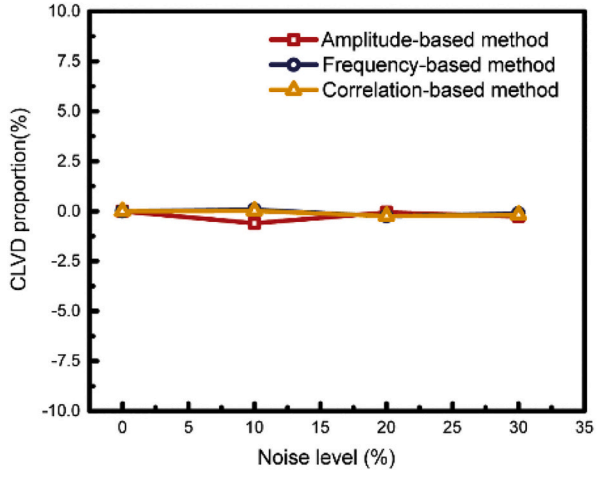

(e) Average value of CLVD component

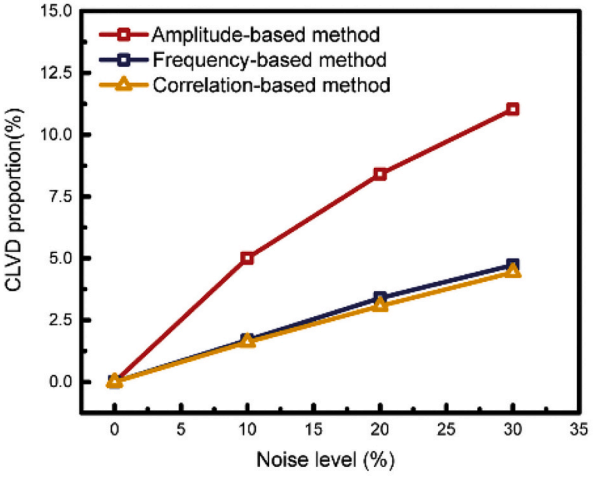

(f) Standard deviation of CLVD component

Fig. 5. For shear cracks, inversion results of the three methods for four noise levels. The correct values of ISO, DC and CLVD proportions are 0%, 100% and 0% respectively.

$$u_n(\mathbf{x},t) = \frac{r_n}{4\pi\rho\alpha^3}\frac{1}{R}(r_1\ r_2\ r_3)\begin{pmatrix} M_{11} & M_{12} & M_{13} \\ M_{12} & M_{22} & M_{23} \\ M_{13} & M_{23} & M_{33} \end{pmatrix}\begin{pmatrix} r_1 \\ r_2 \\ r_3 \end{pmatrix}\dot{S}(t), \tag{2}$$

where, $u_n(\mathbf{x}, t)$ is the displacement in the nth direction, r_1, r_2, r_3 is the direction cosine from source to sensor, $\mathbf{x}$ is the location of sensor and t is the time, ρ is the density of media and α is the P-wave velocity, R is the source-sensor distance and $S(t)$ is the source-time function, which describes the time-dependent opening state of crack surfaces. For the amplitude method, the source-time function is regarded as a step function and $u_n(\mathbf{x}, t)$ is replaced by the amplitudes of waveforms, then the time dependence of Eq. (2) can be ignored. A linear and time-independent algorithm to solve moment tensors can be obtained as:

$$\mathbf{U} = \mathbf{Gm}, \tag{3}$$

where, $\mathbf{U}$ is the column vector containing the measured wave amplitudes. $\mathbf{G}$ is the structure response matrix. $\mathbf{m}$ is the vector containing the unknown moment-tensor components in the form of column vector.

Based on Eq. (3), the least-square solutions of moment tensors can be calculated and the source types can be determined by the decomposition of moment tensors into the three basic components: isotropic (ISO), double-couple (DC) and compensated linear vector dipole (CLVD) (Vavryčuk, 2015). A moment tensor can be written as an orthonormal form as follows:

$$\mathbf{M} = M_1\mathbf{e}_1\mathbf{e}_1 + M_2\mathbf{e}_2\mathbf{e}_2 + M_3\mathbf{e}_3\mathbf{e}_3, \tag{4}$$

where $M_1 > M_2 > M_3$ and vectors $\mathbf{e}_1$, $\mathbf{e}_2$ and $\mathbf{e}_3$ define the tensile, neutral and pressure axes, respectively. Then the moment tensor $\mathbf{M}$ can be written as a linear combination of the three basic components:

$$\mathbf{M} = M_{\mathrm{ISO}}\mathbf{E}_{\mathrm{ISO}} + M_{\mathrm{DC}}\mathbf{E}_{\mathrm{DC}} + M_{\mathrm{CLVD}}\mathbf{E}_{\mathrm{CLVD}}, \tag{5}$$

where $\mathbf{E}_{\mathrm{ISO}}$, $\mathbf{E}_{\mathrm{DC}}$ and $\mathbf{E}_{\mathrm{CLVD}}$ are the ISO, DC and CLVD elementary tensors. Then the relative scale factors C_{ISO}, C_{DC} and C_{CLVD} are defined as:

$$\begin{bmatrix} C_{\mathrm{ISO}} \\ C_{\mathrm{DC}} \\ C_{\mathrm{CLVD}} \end{bmatrix} = \frac{1}{M}\begin{bmatrix} M_{\mathrm{ISO}} \\ M_{\mathrm{DC}} \\ M_{\mathrm{CLVD}} \end{bmatrix}, \tag{6}$$

where, $M = |M_{\mathrm{ISO}}| + |M_{\mathrm{DC}}| + |M_{\mathrm{CLVD}}|$. Source types can be determined by the relative scale factors (Vavryčuk, 2015).

2.2. Correlation-based inversion approach

For the moment tensor inversion, the waveforms recorded by sensors can be distorted by noise or the signals from other sources. This results in errors in the recorded waveform amplitudes used to invert for a single source, leading to noisy inversions with high errors in the solutions. The way to solve this problem is to extract the signals from the contaminated

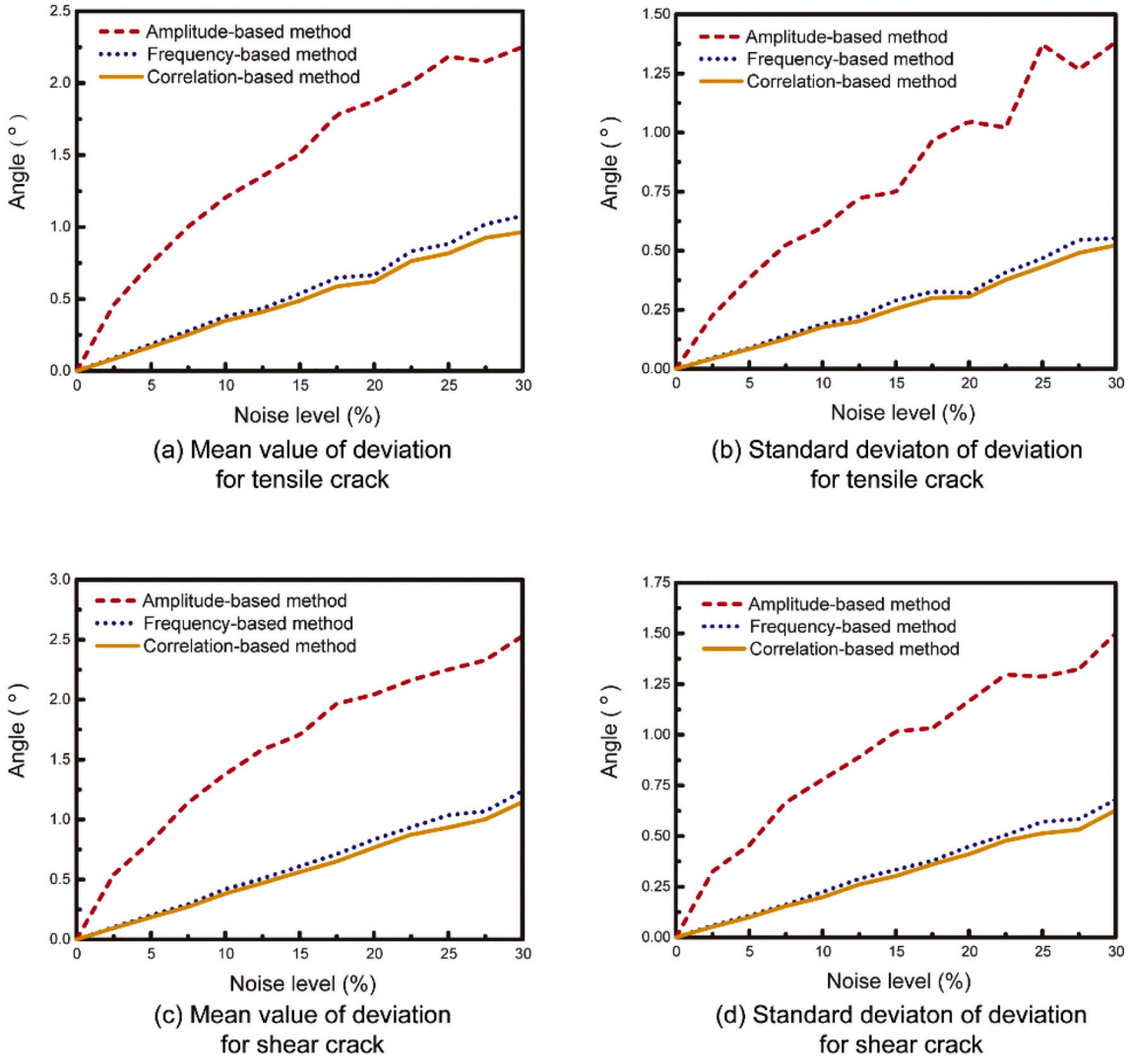

Fig. 6. Deviations of the P/T axes of inversion results. The deviations are defined as the angles between the correct and retrieved P/T axes in degrees.

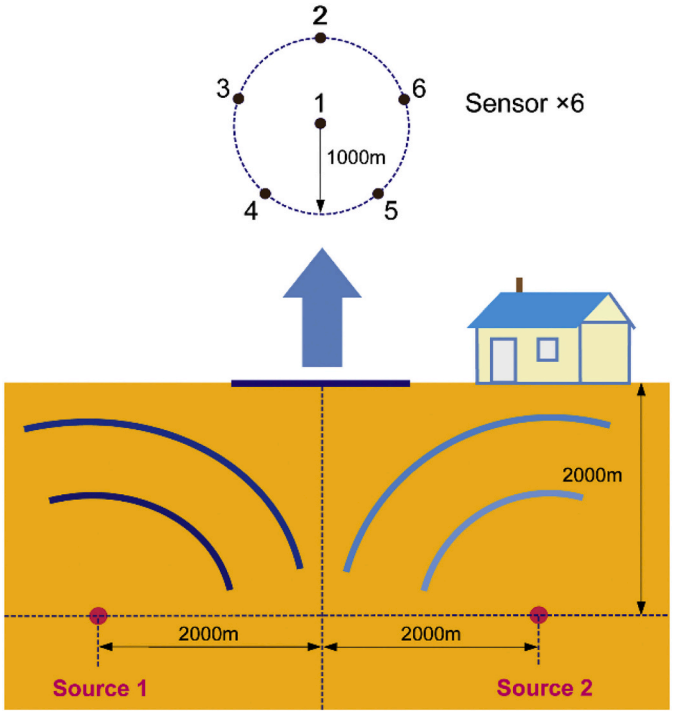

Fig. 7. Configuration of sensors and relative positions between the two sources and sensors.

waveforms. Based on the difference of the frequency spectra of waveforms, signals can be distinguished by Fourier transform. However, Fourier transform is still computationally demanding. Actually, the moment tensor inversion uses the relative amplitudes of waveforms at different locations to identify specific source types and the amplitudes are not the primary interest. Thus, the extracting process for signals can be achieved in a simpler way, which is the waveform-correlation process to be put forward next.

For the waveform-correlation analysis, correlation functions need to be defined first. According to the Green's function (Aki and Richards, 2002), the waves generated by sources are determined by source-time functions, thus correlation functions defined by source-time functions are sensitive to signals and insensitive to noise. Then, the correlation computation between correlation functions and waveforms can filter noise and suppress its effect on the moment tensor inversion for any source types. For engineering applications, source-time functions can be obtained by the waveform analysis (Kravanja et al., 1999), which makes the definition of the correlation functions feasible.

According to Eq. (2), the seismic waves are the time derivative of source-time functions (Aki and Richards, 2002), then the correlation functions can be defined as:

$$F(t_r, t) = \begin{cases} \dot{S}(t - 2nt_r) & 2nt_r \le t \le (2n+1)t_r \\ -\dot{S}(t - (2n+1)t_r) & (2n+1)t_r \le t \le (2n+2)t_r \end{cases} \quad n = 0, 1, 2\ldots, \tag{7}$$

where $F(t_r, t)$ is the correlation function, $S(t)$ is the source-time function, t_r is the duration time and determines the frequency spectra of the correlation functions. The typical source-time function, wave signal and correlation function are plotted in Fig. 1.

As shown in Fig. 1, the shape of correlation functions is similar to that of signals, but t_r can be different from T_r and particular values can be used to realize different functions. For extracting different components from waveforms, the correlation coefficients can be introduced and calculated by the equation as follows:

$$a_r(t_r) = \sum_{i=1}^{n} F(t_r, t_i) u(t_i), \tag{8}$$

where $a_r(t_r)$ is the correlation coefficient corresponding to the duration time t_r. $u(t_i)$ is the effective slice of waveforms.

Because the moment tensor inversion is dependent on the relative amplitudes of the wave signals recorded by different sensors, rather than the absolute amplitudes, correlation coefficients can replace the amplitudes of waves to calculate moment tensors. The linear inversion approach based on correlation coefficients is expressed as follows:

$$\mathbf{A} = \mathbf{Gm}, \tag{9}$$

where $\mathbf{A}$ is the vector whose components are the correlation coefficients $a_r(t_r)$.

When the seismic data are contaminated by noise or the waveforms are the superposition of signals generated by multiple sources, the solutions can be calculated by Eq. (9). The inversion accuracy of the new approach will be evaluated by synthetic tests.

3. Synthetic tests

3.1. Suppressing effect of noise

3.1.1. Synthetic model

For evaluating the performance of the new inversion approach, the synthetic tests are carried out. The moment tensor inversion accuracy can be affected by many factors, e.g., anisotropy, attenuation, source location, numbers and positions of sensors. The effect of these factors on the moment tensor inversion has been studied in detail (Dufumier and Rivera, 1997; Eyre and Van Der Baan, 2017; Silený, 2009; Vavryčuk, 2006). In this study, data processing is the primary interest and the synthetic model is as simple as possible. The seismic data are contaminated by random noise of uniform distribution. It is indeed that real seismic data are more suitable than synthetic data for evaluating the performance of the method. For the lack of real seismic data, synthetic data are used in this study. Synthetic seismic data are calculated according to the Green's function and contains the information of sources. Theoretically, synthetic seismic data can be used for the moment tensor inversion and evaluating the performance of the method.

In the synthetic model, the sensors are arranged on the ground. The depth of the source is 2000 m and the radius of the region, in which sensors are deployed, is 1000 m. The size of the model is defined according to hydraulic fracturing treatments. The configuration of sensors is shown in Fig. 2(a), which has excellent performance of suppressing the effect of noise on the moment tensor inversion (Kong et al., 2019). The direction of the source is shown in Fig. 2(b), in which $\mathbf{n}$ is the normal vector to the crack surfaces and [$\mathbf{l}$] is the slip vector at the crack surfaces.

Tensile and shear cracks are two basic source types and most cracks can be expressed as the combination of the two kinds. Consequently, the correlation-based inversion approach is tested by the two basic sources. For all sources, the vector $\mathbf{n}$ is vertical and unchanged. For tensile cracks, the angle is $\alpha = 90^\circ$ and the angle is $\alpha = 0^\circ$ for shear cracks.

The medium is isotropic and homogeneous, and the material parameters are listed in Table.1. The values are the averages of those of several popular rocks (Schön, 2016). Commonly, the velocity models used in the inversion are much more complicated, but a very simple one is used in this study. Actually, the correlation-based method focuses on data processing and noise filtering, thus the performance of the method is insensitive to velocity models. For simplicity, the velocity model used in this study is simple.

The synthetic seismic data are computed by the Green's function (Aki and Richards, 2002). The authenticity of the seismic data is dependent on source-time functions and the source-time function implemented in this study is expressed according to Ohtsu (1988) as:

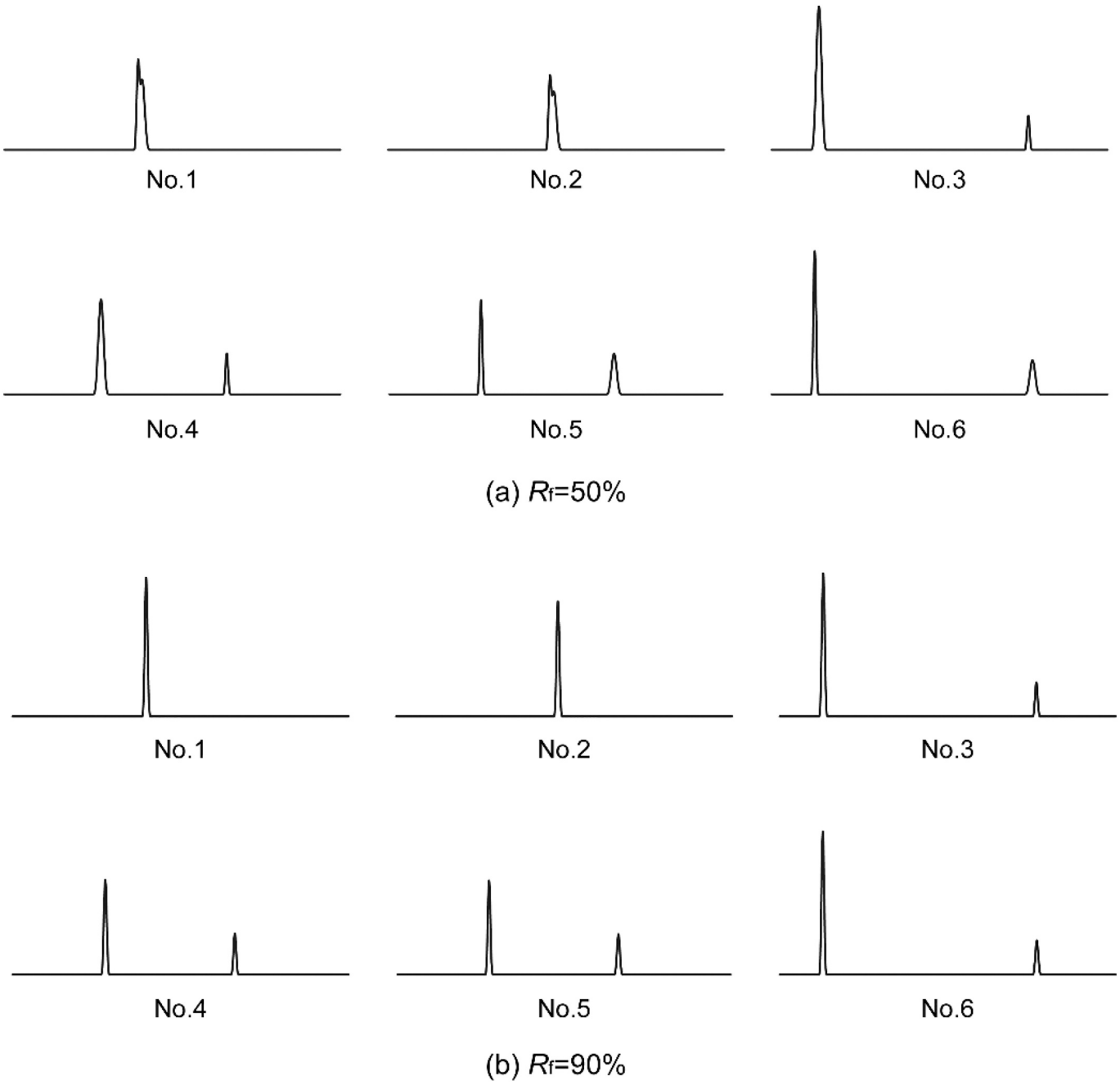

Fig. 8. Waveforms recorded by the sensors for the two-source models. The ratios between the rise times of the two sources are R_f = 50% and 90%.

$$S(t) = \begin{cases} \dfrac{t}{T_r} - \dfrac{2}{3\pi} sin\left(\dfrac{2\pi t}{T_r}\right) + \dfrac{1}{12\pi} sin\left(\dfrac{4\pi t}{T_r}\right) & t < T_r \\ 1 & t \geq T_r \end{cases}, \tag{10}$$

where T_r is the rise time. This source-time function is validated to describe the opening state of actual crack surfaces. The rise time used in this section is 10^{-2} s, which is large for microseismicity. Logically, according to Fig. 1 and Eq. (8), the performance of the correlation-based method is dependent on the relative size between rise and duration times. In the synthetic tests, the inversion results are all expressed by the ratios between rise and duration times, and the value of the rise time has no influence on the conclusions. In addition, if the rise time is too small, the sampling rate of signals is small and the amount of data will be very large, which is computationally demanding. Consequently, a relatively large rise time is used and the conclusions are still suitable for microseismicity.

The synthetic seismic data are mixed with various levels of white noise. The noise is uniformly distributed within the interval and the interval range is proportional to the amplitudes of signals. The noise level is represented by the ratio and the ratios used in this study are 0%, 10%, 20% and 30%. Theoretically, for noise filtering, if the duration time of the correlation function is equal to the rise time of the source-time function, the correlation-based method can achieve the best inversion accuracy. For real data, the rise time can be estimated, but the estimation may be imprecise. A series of correlation functions with sequential duration times can attempt to calculate the correlation coefficients and the one with the maximum absolute value is used to invert for moment tensors. In addition, the effect of rise time on inversion

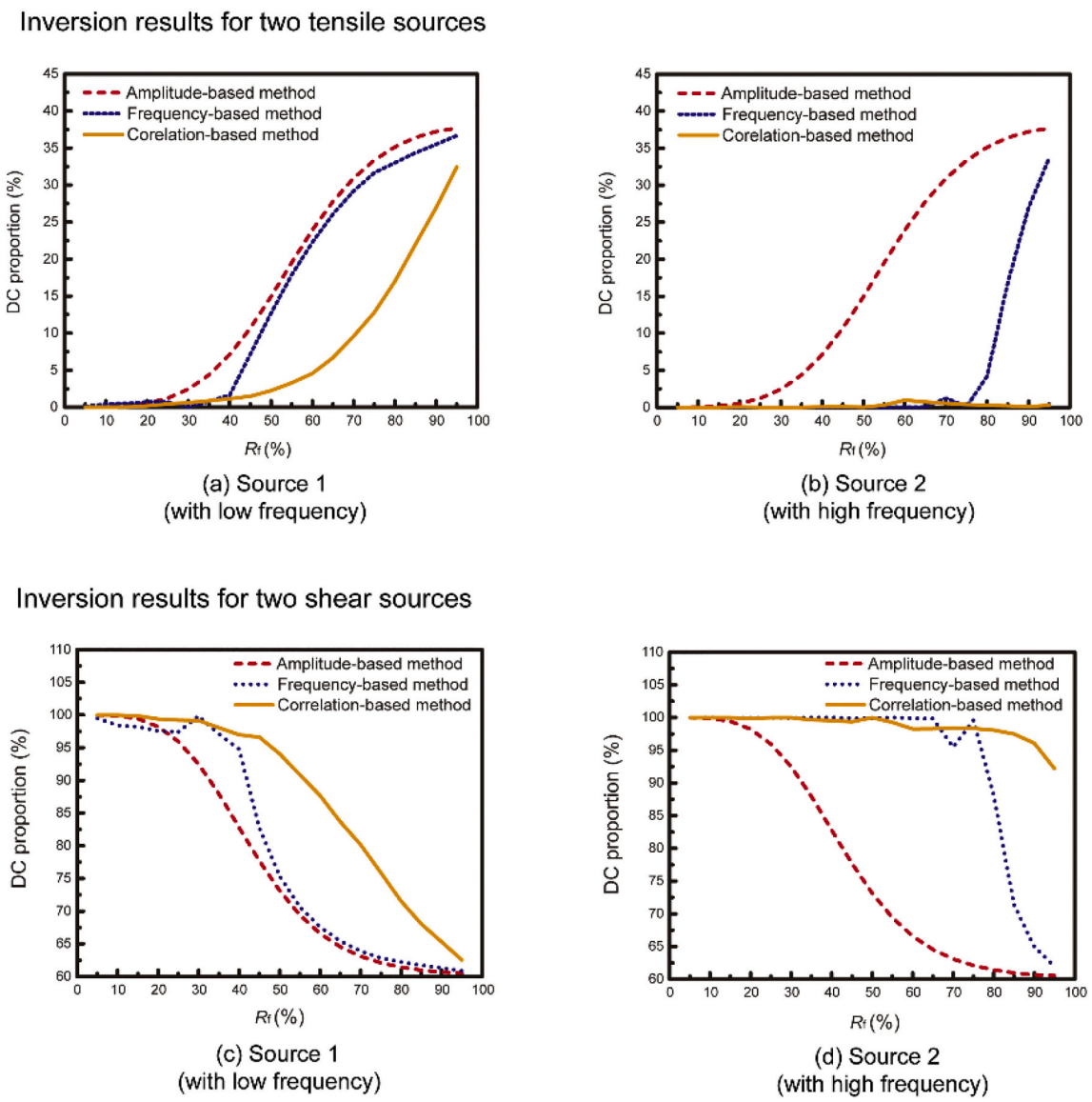

Fig. 9. Inversion results of DC proportions for various relative frequencies between the two sources. $R_f = f_1/f_2 = T2\ r/T1\ r$ is the ratio between the two frequencies. The two sources are pure tensile or shear, and the correct DC proportions are 0% or 100% respectively.

accuracy is analyzed in Section 4.1.1. For the noise level of 30%, the distorted waveforms are plotted in Fig. 3.

3.1.2. *Inversion results*

Under each noise level, the inversion is repeated 100 times to stabilize the inversion results and avoid occasional errors. The accuracy is quantified by the average of the 100 inversion results and the standard deviations of the results are also provided. Two basic source types, which are pure tensile and shear cracks, are used for the inversion. According to Fig. 2, the tensile dislocation is along the normal direction **n** and the angle is $\alpha = 90^\circ$, and the shear dislocation is horizontal and the angle is $\alpha = 0^\circ$.

For the tensile dislocation, the inversion results are plotted in Fig. 4. For comparison, the results calculated by the amplitude-based and frequency-based methods are provided. The amplitude-based method is the commonly-used method and the amplitudes of waveforms are picked up to invert for moment tensors. For the frequency-based method, the time-dependent waveforms are transformed into the frequency domain by Fourier transform and the dominant frequency components are picked out to invert for moment tensors. Because of the difference of the spectrum between signals and noise, the frequency-based method can filter noise and improve the inversion accuracy.

As shown in Fig. 4, the inversion errors of DC and CLVD proportions are sensitive to noise and increase with the increase of noise levels. The ISO proportions are unchanged for different noise levels. The standard deviations for the three components increase with the increase of noise levels. Although inversion errors are inevitable, the errors for the correlation-based method are less than half of those for the amplitude-based method. The inversion accuracy of the correlation-based method is similar to that of the frequency-based method, but it should be noted that the correlation-based method is much simpler and requires less computing resources. Consequently, the correlation-based method still has advantages.

Most cracks are not pure tensile or shear cracks, but can be expressed as the combinations of the two basic sources. For evaluating the general applicability of the correlation-based method, the inversion results for shear cracks are provided. According to Fig. 2(b), the shear dislocation is horizontal and the angle is $\alpha = 0^\circ$. The ISO, DC and CLVD proportions of

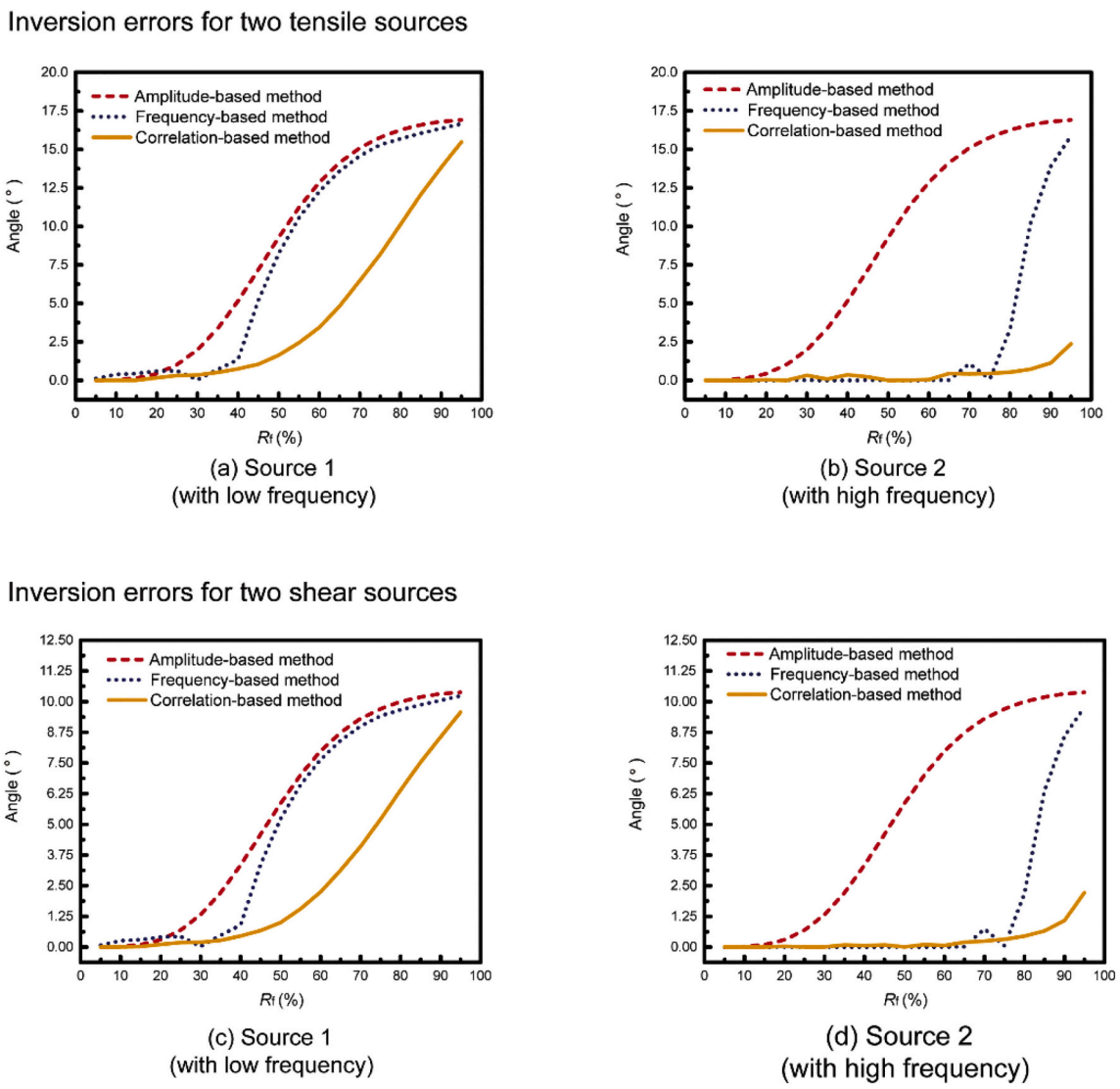

Fig. 10. Deviations of P/T axes for various relative frequencies between the two sources. The deviations are defined as the angles between the correct and retrieved axes in degrees.

the retrieved moment tensors are plotted in Fig. 5.

As shown in Fig. 5, the correlation-based inversion method is effective for shear cracks and the improvement of inversion accuracy can be more than 50%, which is similar to that for tensile cracks. The errors of the three components for shear cracks are smaller than those for tensile cracks at the same noise level. Because shear-tensile cracks can be expressed as the combinations of tensile and shear cracks, it is logical that the correlation-based method is also suitable for shear-tensile sources.

For the sources in the synthetic tests, the fault surfaces are horizontal. For evaluating the inversion errors of directions, the deviations of P/T axes are plotted in Fig. 6. The deviations are defined as the angles between the correct and retrieved P/T axes in degrees. The deviations for tensile and shear cracks are provided, and the mean values and standard deviations of the repeated inversion results are plotted.

As shown in Fig. 6, the retrieved P/T axes of the inversion results of the correlation-based method are smaller than those of the amplitude-based method. The performance of the method for tensile and shear cracks is similar. According to the inversion results, it can be concluded that the correlation-based method are effective to suppress the effect of noise on the moment tensor inversion in a simple way.

3.2. *Discrimination of multiple sources*

3.2.1. *Double sources model*

In some cases, the waveforms recorded by sensors contain the signals from multiple sources and the amplitudes for each source can not be picked up. Then the amplitude-based method can not result in accurate solutions. In this case, the correlation-based inversion method can be used.

In order to test the performance of the correlation-based inversion method for discriminating multiple sources, a numerical model with two sources is used and illustrated in Fig. 7. The depths of sources, source types, configuration of sensors and medium are the same as those of the single-source model in Fig. 2. The waveforms recorded by the sensors No.1 and 2 are the superposition of the signals generated by the sources 1 and 2. The source types used in the synthetic tests are pure tensile and shear. For simplicity, the two sources initiate at time 0 s simultaneously, which is a rare but extreme situation. The effect of the time delay between the two events is analyzed in Section 4.2.2.

Obviously, for discriminating multiple sources, the performance of the new inversion approach is dependent on the relative magnitude between the rise times of two sources and the selected correlation

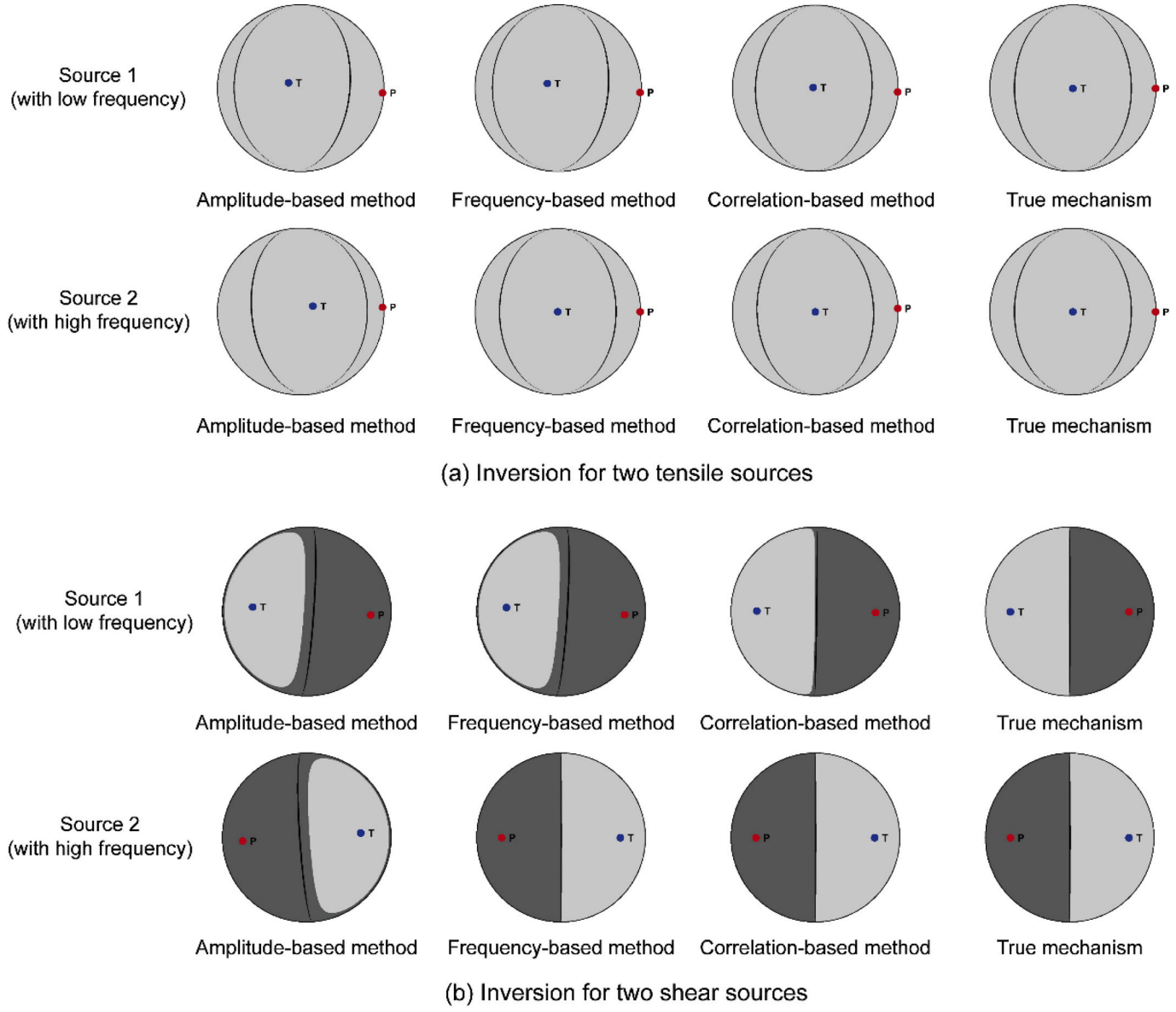

Fig. 11. 'Beach balls' of the sources for $R_f = 50\%$.

functions for different sources. Commonly, seismic waveforms are characterized by frequencies, rather than rise times. Because seismic waves always have broadband, the dominant frequency defined as $1/T_r$ is used for engineering applications. Thus the frequency characteristic is represented by the dominant frequency.

The rise time for source 2 is 10^{-2} s (the corresponding dominant frequency is 10^2Hz) and unchanged. In the synthetic tests, various frequencies of source 1 are used, but the waveforms are similar that the waveforms recorded by No.1 and 2 are the superposition of the two signals and the other waveforms are not. It should be noted that the rise times are large for microseismicity. According to theoretical analysis, the performance of the method for multiple source discrimination is dependent on relative frequency between the two sources. The values of rise times have no influence on the performance of the method. In addition, if the rise times are too small, the amount of data can be very large and more computational resources are needed. Consequently, relative large rise times are used in the synthetic tests.

3.2.2. *Inversion results for two sources*

For superimposed waveforms, the spectrum is easier to obtain than the rise time. Consequently, the frequency is used for characterizing signals and defined as the reciprocal of the rise time. For the generality of the conclusions, the frequency of source 1 (low frequency and denoted as f_1) is set to be proportional to that of source 2 (high frequency and denoted as f_2), and the ratio is defined as $R_f = f_1/f_2 = T2\ \mathrm{r}/T1\ \mathrm{r}$. The representative waveforms recorded by the sensors for $R_f = 50\%$ and 90% are plotted in Fig. 8.

The correlation functions with proper duration times or inversion frequencies are used to calculate the correlation coefficients and the moment tensors are recovered. The proper inversion frequencies correspond to the minimum inversion errors and the values will be discussed in Section 4.2.1. The inversion errors are plotted in Figs.9 and 10. Fig. 9 illustrates the inversion errors of DC proportions and Fig. 10 illustrates the deviation of P/T axes. The deviation of P/T axes is defined as the angle between the correct and retrieved P/T axes by degree. Two cases of two tensile cracks and two shear cracks are studied. According to Fig. 2(b), the angles are $\alpha = 90^\circ$ for the two tensile sources. In should

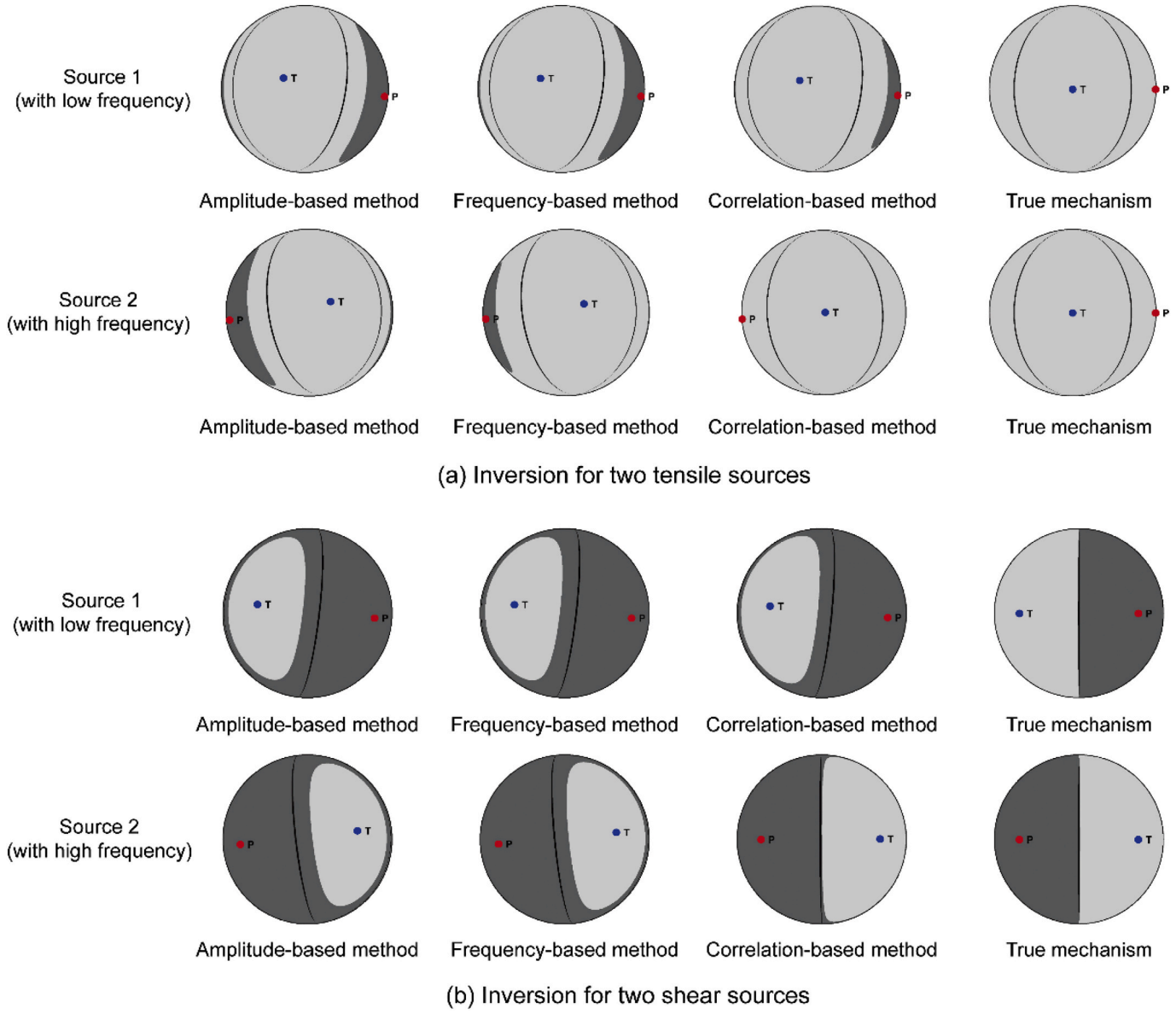

Fig. 12. 'Beach balls' of the sources for $R_f = 90\%$.

be noted that the slip orientations of the two shear sources are different. The angle is $\alpha = 180^\circ$ for source 1 and the angle is $\alpha = 0^\circ$ for source 2.

As shown in Figs.9 and 10, the inversion errors of the correlation-based method are much smaller than those of the amplitude- and frequency-based methods, which indicates the superiority of the correlation-based method. In addition, although the error values vary for different source types, the performance of improving inversion accuracy is similar to each other, which indicates the effectiveness of the method for different source types. Moreover, the shapes of the curves of DC proportions are in agreements with those of P/T deviations.

For visually illustrating the source mechanisms, the 'beach balls' for the ratios of $R_f = 50\%$ and 90% are plotted in Figs.11 and 12.

As shown in Figs.11 and 12, the inversion errors for $R_f = 50\%$ and 90% are different. Specifically, the performance of the correlation-based method is dependent on the relative frequencies of the two sources. For the source with low frequency (Fig. 9 (a) (c) and Fig. 10 (a) (c)), the advantage of the correlation-based method is in the relative frequency range of $40\% < R_f < 90\%$. When the frequencies of the two sources are too close to each other ($R_f > 90\%$), the inversion errors for the correlation-based method are great, but still smaller than those for the other two methods. For the source with high frequency (Fig. 9 (b) (d) and Fig. 10 (b) (d)), the correlation-based method is effective regardless of the relative frequencies.

It should be noted that the correlation-based method is only suitable for multiple tensile sources or some particular cases (e.g. the two shear sources in this section). In other cases, for a sensor, the first-motion directions of the recorded signals from different sources may be opposite. If the waveforms are the superpositions of those signals, the recorded signals cancel each other and some signal components disappear. In those cases, the correlation-based method can not calculate the accurate solutions and the inversion errors are great. The reason is the inefficiency of the correlation functions used in this study and some other correlation functions should be defined to solve this problem.

For engineering applications, the precise characteristics of sources are unknown before the moment tensor inversion. It is recommended that the correlation-based method with the correlation function of Eq. (7) should be used for the cases in which tensile cracks are the majority. For hydraulic fracturing treatments, tensile cracks are quite common

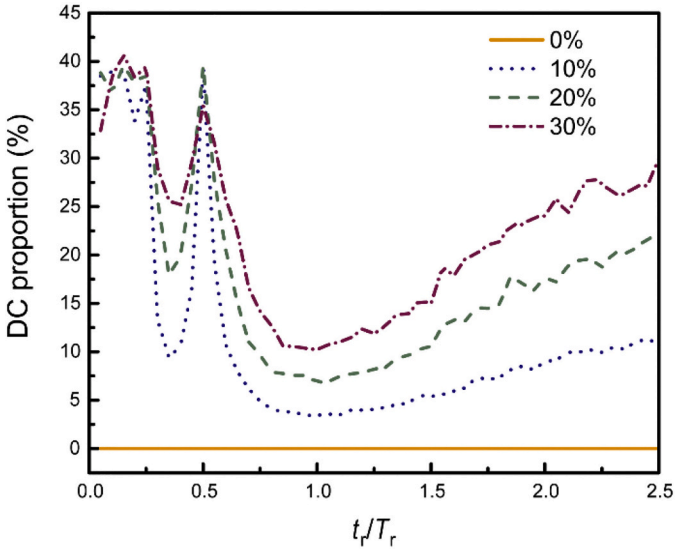

Fig. 13. Inversion results for the correlation-based method for various duration times. t_r is the duration time and T_r is the rise time. Four curves correspond to the noise levels. The correct DC proportion is 0%.

and the method can work. For other engineering applications, this method need further researches to be used.

4. Discussion

In Section 3, the performance of the correlation-based method for noise filtering and multiple sources discrimination is illustrated. In those synthetic tests, the parameters are preset. For generality, the influence of some parameters need further discussions. For noise filtering, two parameters are studied, which are the difference between the rise and duration times, and the number of sensors. For multiple sources discrimination, the proper inversion frequencies and time delay between the two events are discussed.

4.1. Parameter influence for noise filtering

4.1.1. Difference between rise and duration times

According to the analysis in Section 3.1, the correlation-based method can achieve the best performance of noise filtering, when the duration time is equal to the rise time. For engineering applications, the source-time function can be retrieved, but the estimated rise time of the source-time function may be imprecise. Then, for the moment tensor inversion, the duration time may be different from the correct rise time and the performance of the method is affected. Thus, the influence of the rise time on the inversion accuracy is studied in this section.

For rise times, the performance of the correlation-based method is dependent on the relative amplitudes between rise and duration times. Consequently, for generality, duration times used for the inversion are defined proportional to rise times. According to the synthetic tests in Section 3.1, the correlation-based method for noise filtering is suitable for tensile and shear cracks, thus pure tensile cracks are used for illustration. The DC proportion of the moment tensor of a pure tensile crack is 0, which is helpful for comparison. At four noise levels, the inversion errors for various duration times are plotted in Fig. 13. The horizontal axis is defined as the ratio t_r/T_r, which t_r is the duration time and T_r is the rise time.

As shown in Fig. 13, when the duration time t_r is equal to the rise time T_r ($t_r/T_r = 1$), the correlation-based method can achieve the best performance of suppressing the effect of noise. If the duration time is half of the rise time ($t_r/T_r = 0.5$), inversion error is great and this value should be avoided. When the duration time is larger than the rise time, the error increases gradually. According to the inversion results in Fig. 4, when the duration time is in the range $0.7 < t_r/T_r < 1.8$, the inversion results obtained by the correlation-based method are more accurate than those obtained by the amplitude-based method. This interval is relatively wide and the correlation-based method is practical for engineering applications.

4.1.2. Numbers of sensors

For the moment tensor inversion, six to-be-solved moment-tensor components require at least six sensors to avoid an underdetermined problem. For engineering applications, more sensors are commonly used to improve the inversion accuracy. Consequently, the performance of the correlation-based method for different numbers of sensors should be studied.

For comparison, a configuration of 11 sensors is used for the moment tensor inversion. The 11 sensors are deployed as a star shape and the configuration is shown in Fig. 14(b).

For the configuration of 11 sensors in Fig. 14(b), 5 extra sensors (No.7, 8, 9, 10, 11 sensors) are added on the circular of the radius of 500 m. The relative positions between the sensors and source are the same as that in Fig. 2(a). The source type is pure tensile and the angle is $\alpha = 90^\circ$. The moment tensor is inverted by synthetic seismic data and the ISO, DC and CLVD proportions are plotted in Fig. 15.

As shown in Fig. 15, the inversion results for 11 sensors are similar to those for 6 sensors. Compared with the amplitude-based method, the correlation-based method can improve the inversion accuracy and the improvement is more than 50%. The results indicate that the

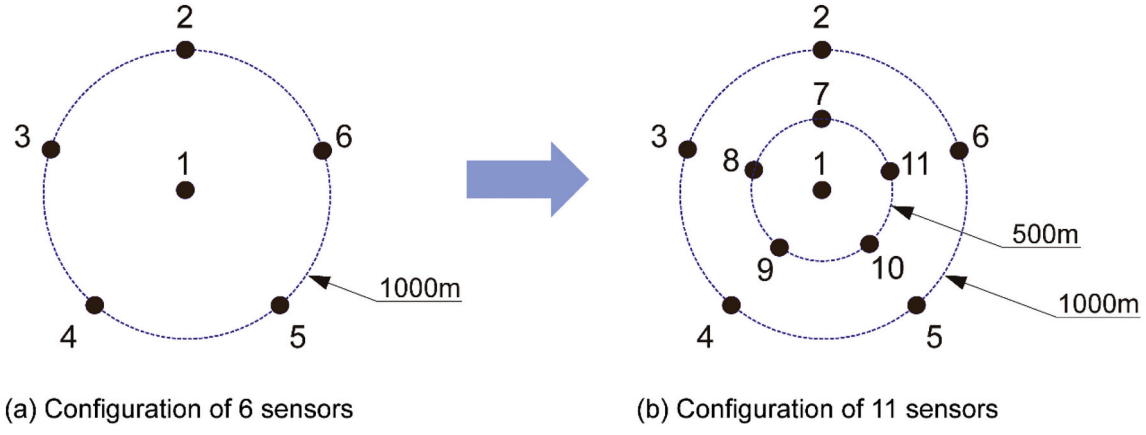

Fig. 14. Configurations of 6 and 11 sensors. The sensors are represented by the black dots and deployed as a star shape.

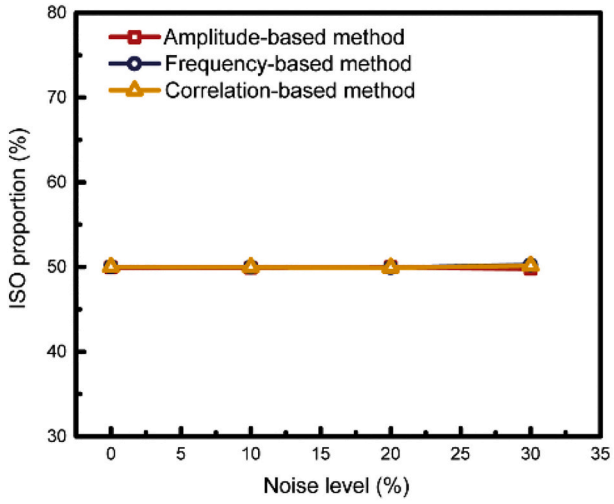

(a) Average value of ISO component

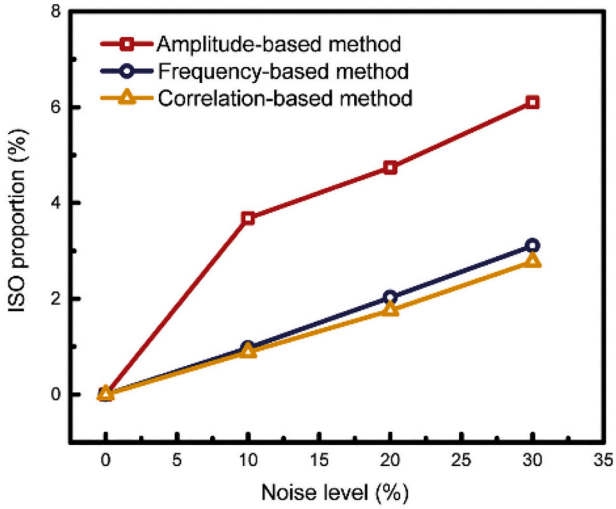

(b) Standard deviation of ISO component

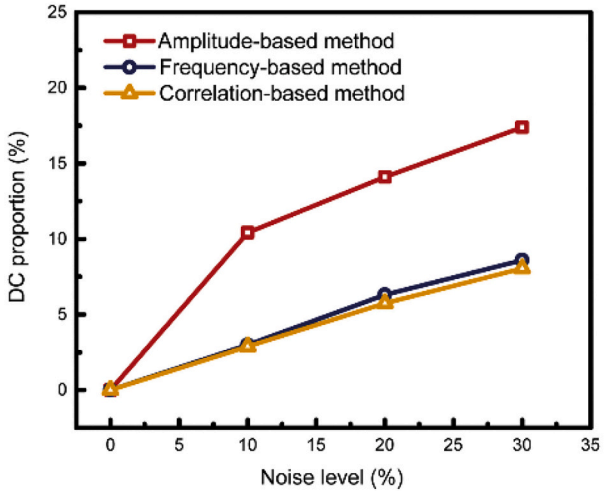

(c) Average value of DC component

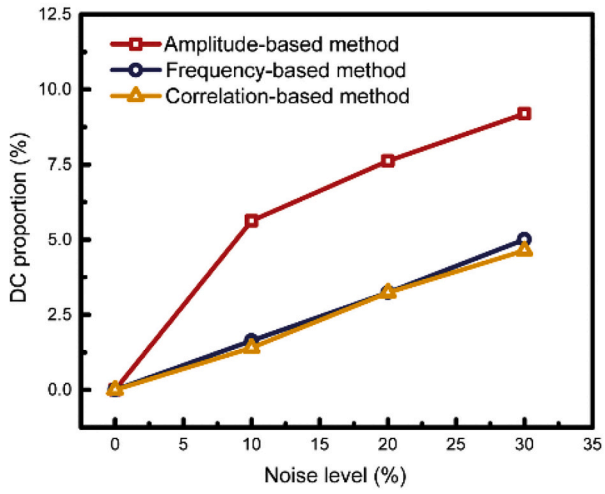

(d) Standard deviation of DC component

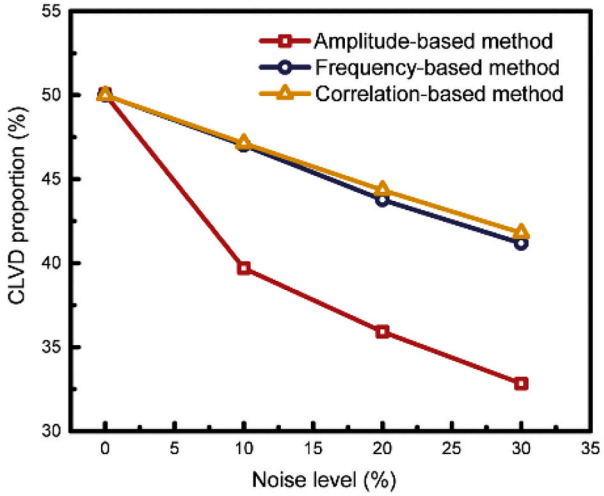

(e) Average value of CLVD component

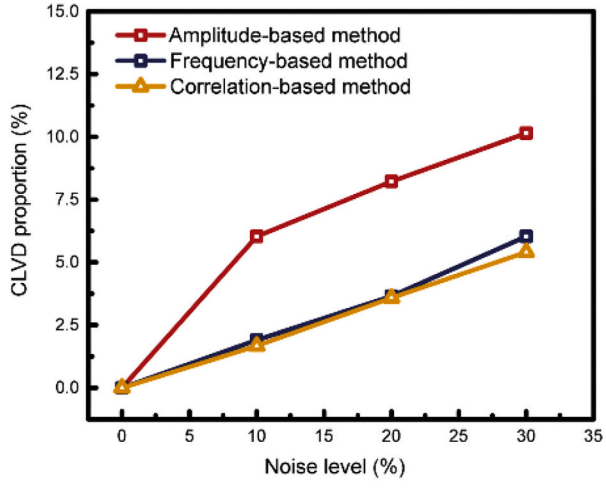

(f) Standard deviation of CLVD component

Fig. 15. ISO, DC and CLVD proportions of the moment tensors inverted by 11 sensors. The correct values of the three proportions are 50%, 0% and 50% respectively.

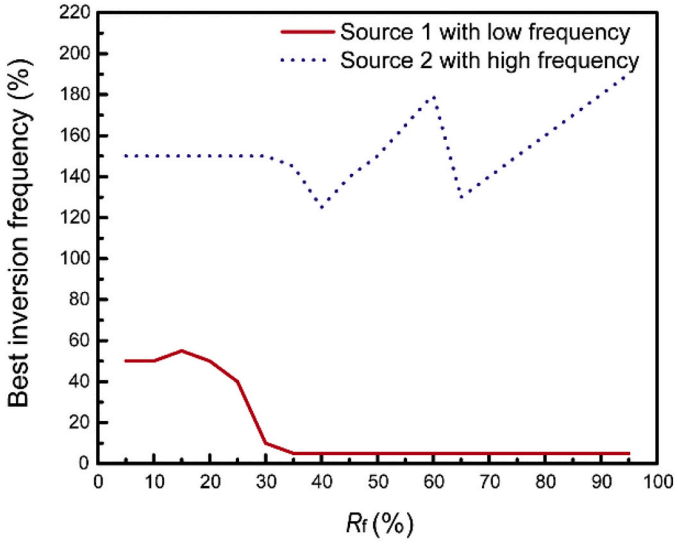

Fig. 16. Best inversion frequencies of the correlation functions for the two sources. $R_f = f_1/f_2 = T2\ r/T1\ r$ is the relative frequencies between the two sources. For each source, the inversion frequencies are expressed as the proportions to the frequency of the source. The rise time is transformed to the inversion frequency by the relation $1/(T_r)$ and the duration time is transformed to the frequency of the source by the relation $1/(2t_r)$.

correlation-based method is effective for 11 sensors and the performance is similar to that of 6 sensors. Consequently, it can be concluded that the numbers of sensors do not affect the performance of the new method. In addition, the inversion results also indicate that more sensors are helpful for improving the inversion accuracy.

4.2. Parameter influence on multiple sources discrimination

4.2.1. Inversion frequency

For noise filtering, the duration time of the correlation function should be as close to the rise time as possible to achieve the best performance. However, for discriminating multiple sources, the duration time for the best performance may not be equal to the rise time and should be determined separately. In this section, the best duration time is discussed and determined by the synthetic tests.

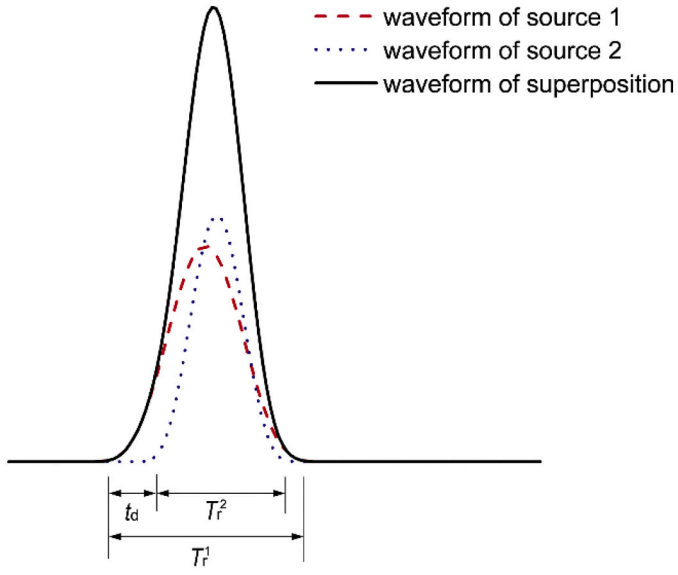

Fig. 17. Relative amplitude between the time delay and rise times. t_d is the time delay between the two events, $T1$ r and $T2$ r are the rise times of the two sources.

For superimposed signals, the spectrum is easier to obtain than the rise time. Consequently, we calculate the best inversion frequency rather than the best duration time. The duration time is transformed to the inversion frequency based on the relation $1/(2t_r)$ and the frequency of the source is the reciprocal of the rise time as $1/T_r$. The inversion frequency for the minimum inversion error is denoted as the best inversion frequency. According to the synthetic tests, the best inversion frequencies are expressed as the proportions to the frequencies of the sources and plotted in Fig. 16.

As shown in Fig. 16, for the source with low frequency, if the frequency difference between the two sources is quite large ($R_f < 30\%$), the best inversion frequency is large. Actually, under these circumstances, all inversion frequencies are suitable for the inversion, as long as the inversion frequency is smaller than the frequency of the source. When the frequencies of the two sources get close to each other, the best inversion frequency for source 1 (with low frequency) should be as small as possible. For the source with high frequency, the best inversion frequency varies with the change of relative frequencies of the two sources.

According to the spectrum of the superimposed waveforms, the frequencies of the two sources can be obtained. Based on Fig. 16, the best inversion frequencies of the correlation functions can be determined for the moment tensor inversion. Then, the accurate moment tensors of the two sources can be calculated by the correlation-based method.

4.2.2. Time delay between two events

For the synthetic tests in Section 3.2, the two events initiate at the same time. Actually, for engineering applications, this situation is rare and the nonzero time delays between the two events are more common. Consequently, the analysis for the effect of time delays on the performance of the correlation-based method is carried out.

The time delay is defined in Fig. 17, in which t_d is the time delay between the two events, and $T1$ r and $T2$ r are the rise times of the two sources.

For the synthetic tests, the ratios between the rise times are $R_f = T2\ r/T1\ r = 80\%$ and 90%, because the inversion errors are great in those cases. The two sources are pure tensile with the angles being $\alpha = 90^\circ$. The time delay t_d is proportional to the rise time $T1$ r and the inversion errors are plotted in Fig. 18. The inversion results for the ratios of $0 \le t_d/T1\ r \le 50\%$ are provided. When the ratio $t_d/T1\ r > 50\%$, the signals of the two sources can be separated easily and the commonly-used amplitude-based method can be used.

As shown in Fig. 18, for the ratios of $R_f = 80\%$ and 90%, in the range of $0 \le t_d/T1\ r \le 10\%$, the inversion errors are great and the maximum errors are at $t_d/T1\ r = 10\%$ and 5% respectively. With the increase of the ratios of $t_d/T1$ r, the errors are reduced to about 0 sharply. Actually, regardless of the ratios of R_f, when the time delays are very small, the inversion errors are always great. Still, the exact value of $t_d/T1$ r for the maximum error is related to the ratio of R_f. Consequently, for convenience, in the synthetic tests in Section 3.2, the time delay between the two events are 0 and unchanged for the moment tensor inversion.

5. Conclusion

In the moment tensor inversion for hydraulic fractures, the inversion approach based on the amplitudes of waveforms may not provide accurate solutions, because the waveforms recorded by sensors are contaminated by noise, or can be the superposition of signals generated by multiple sources.

In this paper, a new inversion approach is proposed based on the correlation between waveforms and correlation functions. In the new inversion approach, the amplitudes of waveforms are replaced by the correlation coefficients to invert for moment tensors. Correlation

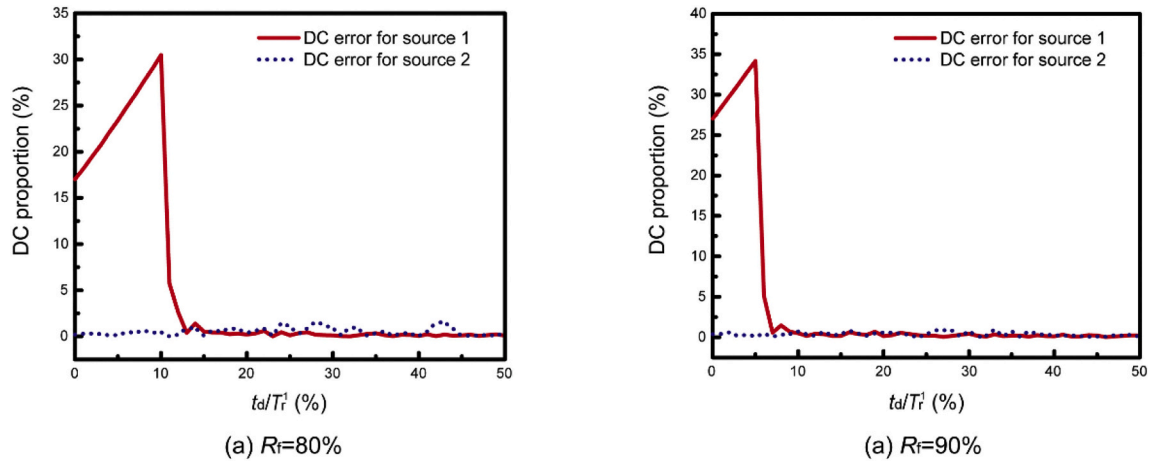

Fig. 18. Inversion results of DC proportions for different time delays t_d. The ratios between the rise times of the two sources are $R_f = T2\ r/\ T1\ r = 80\%$ and 90%. The correct value of DC proportion for the two sources is 0%.

coefficients are computed by the correlation functions, which are defined according to source-time functions. The performance of the correlation-based inversion method is validated by the synthetic tests and the following conclusions are arrived:

1. For noise filtering, the correlation-based method is suitable for tensile and shear sources. Compared with the traditional inversion method, the correlation-based method can improve the inversion accuracy by more than 50% at various noise levels.
1. The correlation-based method can achieve the best performance of noise filtering, when the duration time of the correlation function is equal to the rise time of the source-time function. A small difference between the duration and rise times is tolerable. The effectiveness of the new method is not affected by the number of sensors used in the inversion.
2. For multiple sources discrimination, the correlation-based method can provide accurate solutions for the sources simultaneously. The best inversion frequencies of the correlation functions should be determined separately and the guidelines are provided in Section 4.2.1. Time delays between the two events have a great influence on the performance of the correlation-based method and small time delays result in great inversion errors.

For multiple sources discrimination, the correlation-based method requires that the signals contained in the superimposed waveforms should have the same first-motion direction at the sensor location. Otherwise, the correlation-based method can not calculate accurate moment-tensor solutions. Because the characteristics of sources are unknown before the inversion, the correlation-based method should be used in the cases, in which most cracks are tensile (e.g. microseismicity recorded during hydraulic fracturing) or the above conditions are satisfied. For expanding the application scope of the new method, new correlation functions are needed and the correlation-based method need further researches.

Funding

This work was supported by the Strategic Priority Research Program of the Chinese Academy of Sciences [Grant No. XDA22000000]; and National Natural Sciences Foundation [Grant No. 41804134].

Declaration of competing interest

None.

References

Aki, K., Richards, P.G., 2002. Quantitative seismology. University Science Books, Sausalito, CA.
Baig, A., Urbancic, T., 2010. Microseismic moment tensors: a path to understanding frac growth. Lead. Edge 29, 320–324.
Birialtsev, E.V., Demidov, D.E., Mokshin, E.V., 2017. Determination of moment tensor and location of microseismic events under conditions of highly correlated noise based on the maximum likelihood method. Geophys. Prospect. 65, 1510–1526.
Burridge, R., Knopoff, L., 1964. Body force equivalents for seismic dislocations. Bull. Seismol. Soc. Am. 54, 1875–1888.
Cesca, S., Buforn, E., Dahm, T., 2006. Amplitude spectra moment tensor inversion of shallow earthquakes in Spain. Geophys. J. Int. 166, 839–854.
Dufumier, H., Rivera, L., 1997. On the resolution of the isotropic component in moment tensor inversion. Geophys. J. Int. 131, 595–606.
Dziewonski, A.M., Chou, T.A., Woodhouse, J.H., 1981. Determination of earthquake source parameters from waveform data for studies of global and regional seismicity. J. Geophys. Res. 86, 2825–2852.
Eaton, D.W., Van Der Baan, M., Birkelo, B., Tary, J.-B., 2014. Scaling relations and spectral characteristics of tensile microseisms: evidence for opening/closing cracks during hydraulic fracturing. Geophys. J. Int. 196, 1844–1857.
Eyre, T.S., Van Der Baan, M.V., 2015. Overview of moment-tensor inversion of microseismic events. Lead. Edge 34, 882–888.
Eyre, T.S., Van Der Baan, M., 2017. The reliability of microseismic moment-tensor solutions: surface versus borehole monitoring. Geophysics 82, KS113–KS125.
Fischer, T., Guest, A., 2011. Shear and tensile earthquakes caused by fluid injection. Geophys. Res. Lett. 38.
Fojtíková, L., Vavryčuk, V., Cipciar, A., Madarás, J., 2010. Focal mechanisms of micro-earthquakes in the Dobrá Voda seismoactive area in the Malé Karpaty Mts.(little Carpathians), Slovakia. Tectonophysics 492, 213–229.
Gu, C., Marzouk, Y.M., Toksöz, M., 2017. Bayesian moment tensor inversion and uncertainty quantification for induced seismicity: Uncertainties from both the location and velocity model. In: SEG Technical Program Expanded Abstracts 2017. Society of Exploration Geophysicists, pp. 2784–2790.
Hallo, M., Asano, K., Gallovic, F., 2017. Bayesian inference and interpretation of centroid moment tensors of the 2016 Kumamoto earthquake sequence, Kyushu, Japan. Earth Planets Space 69, 19.
Hardebeck, J.L., Shearer, P.M., 2003. Using S/P amplitude ratios to constrain the focal mechanisms of small earthquakes. Bull. Seismol. Soc. Am. 93, 2434–2444.
Hejrani, B., Tkalcic, H., Fichtner, A., 2017. Centroid moment tensor catalogue using a 3-D continental scale earth model: application to earthquakes in Papua New Guinea and the Solomon Islands. J. Geophys. Res.-Solid Earth 122, 5517–5543.
Hudson, J.A., Pearce, R.G., Rogers, R.M., 1989. Source type plot for inversion of the moment tensor. J. Geophys. Res. 94, 765–774.
Jechumtalova, Z., Eisner, L., 2008. Seismic source mechanism inversion from a linear array of receivers reveals non-double-couple seismic events induced by hydraulic fracturing in sedimentary formation. Tectonophysics 460, 124–133.
Jechumtalova, Z., Silený, J., 2005. Amplitude ratios for complete moment tensor retrieval. Geophys. Res. Lett. 32.
Jian, P.R., Tseng, T.L., Liang, W.T., Huang, P.H., 2018. A new automatic full-waveform regional moment tensor inversion algorithm and its applications in the Taiwan area. Bull. Seismol. Soc. Am. 108, 573–587.
Kanamori, H., Given, J.W., 1981. Use of long-period surface waves for rapid determination of earthquake-source parameters. Phys. Earth Planet. Inter. 27, 8–31.
Kong, Y., Li, M., Chen, W.M., 2019. Sensor arrangement in moment-tensor inversion for cracks. J. Beijing Univ. Aeronautics. 45, 1380–1387 (in Chinese).
Kravanja, S., Panza, G.F., Silený, J., 1999. Robust retrieval of a seismic point-source time function. Geophys. J. Int. 136, 385–394.

Mustac, M., Tkalcic, H., 2017. On the use of data noise as a site-specific weight parameter in a hierarchical Bayesian moment tensor inversion: the case study of the geysers and long valley caldera earthquakes. Bull. Seismol. Soc. Am. 107, 1914–1922.
Nakano, M., Kumagai, H., Inoue, H., 2008. Waveform inversion in the frequency domain for the simultaneous determination of earthquake source mechanism and moment function. Geophys. J. Int. 173, 1000–1011.
Napoli, V.J., Ebel, J.E., 2018. Relative location analysis and moment tensor inversion of the 2012 Gulf of Maine earthquake swarm. Seismol. Res. Lett. 89, 229–240.
Ohtsu, M., 1988. Source inversion of acoustic emission waveform. Doboku Gakkai Ronbunshu 1988, 71–79.
Schön, J.H., 2016. Peysical Properties of Rocks. Petroleum Industry Press, Beijing.
Silený, J., 2009. Resolution of non-double-couple mechanisms; simulation of hypocenter mislocation and velocity structure mismodeling. Bull. Seismol. Soc. Am. 99, 2265–2272.
Silený, J., Panza, G.F., Campus, P., 1992. Waveform inversion for point source moment tensor retrieval with variable hypocentral depth and structural model. Geophys. J. Int. 109, 259–274.
Sipkin, S.A., 1982. Estimation of earthquake source parameters by the inversion of waveform data: synthetic waveforms. Phys. Earth Planet. Inter. 30, 242–259.
Sipkin, S.A., 1986. Interpretation of non-double-couple earthquake mechanisms derived from moment tensor inversion. J. Geophys. Res. 91, 531–547.
Tape, W., Tape, C., 2012. A geometric comparison of source-type plots for moment tensors. Geophys. J. Int. 190, 499–510.
Vackar, J., Burjanek, J., Gallovic, F., Zahradnik, J., Clinton, J., 2017. Bayesian ISOLA: new tool for automated centroid moment tensor inversion. Geophys. J. Int. 210, 693–705.
Van Der Baan, M.V., Eaton, D.W., Preisig, G., 2016. Stick-split mechanism for anthropogenic fluid-induced tensile rock failure. Geology 44, 503–506.
Vavryčuk, V., 2006. Spatially dependent seismic anisotropy in the Tonga subduction zone: a possible contributor to the complexity of deep earthquakes. Phys. Earth Planet. Inter. 155, 63–72.
Vavryčuk, V., 2015. Moment tensor decompositions revisited. J. Seismol. 19, 231–252.
Vavryčuk, V., Hrubcová, P., 2017. Seismological evidence of fault weakening due to erosion by fluids from observations of intraplate earthquake swarms. J. Geophys. Res. Solid Earth 122, 3701–3718.
Vavryčuk, V., Kühn, D., 2012. Moment tensor inversion of waveforms: a two-step time-frequency approach. Geophys. J. Int. 190, 1761–1776.
Vavryčuk, V., Bohnhoff, M., Jechumtálová, Z., Kolář, P., Šílený, J., 2008. Non-double-couple mechanisms of microearthquakes induced during the 2000 injection experiment at the KTB site, Germany: a result of tensile faulting or anisotropy of a rock? Tectonophysics 456, 74–93.
Vavrycuk, V., Adamova, P., Doubravova, J., Jakoubkova, H., 2017. Moment tensor inversion based on the principal component analysis of waveforms: method and application to microearthquakes in West Bohemia, Czech Republic. Seismol. Res. Lett. 88, 1303–1315.
Xu, S.D., Li, Y.H., Liu, J.P., 2017. Detection of cracking and damage mechanisms in brittle granites by moment tensor analysis of acoustic emission signals. Acoust. Phys. 63, 359–367.
Zhang, X.P., Zhang, Q., 2017. Distinction of crack nature in brittle rock-like materials: a numerical study based on moment tensors. Rock Mech. Rock. Eng. 50, 2837–2845.